Molecular imprinting of benzylpiperazine: a comparison of the self-assembly and semi-covalent approaches

Kathleen M. Wright [1,2], **Michael C. Bowyer** [3], **Adam McCluskey** [2] **and Clovia I. Holdsworth** [2,*]

[1] Sanitarium Health Food Company, 1 Sanitarium Drive, Berkeley Vale, NSW 2261, Australia
[2] School of Environmental and Life Sciences, University of Newcastle, Callaghan, NSW 2308, Australia
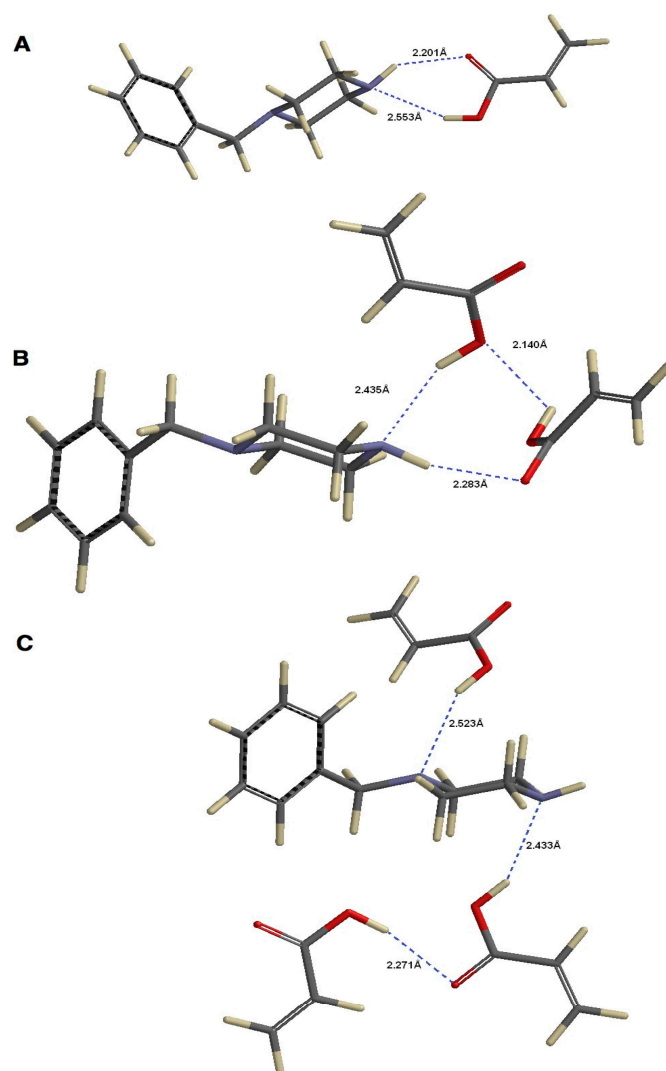[3] Academic Division, University of Newcastle, Ourimbah, NSW 2258, Australia
[*] Correspondence: clovia.holdsworth@newcastle.edu.au; Tel.: +61-2-4921-5481
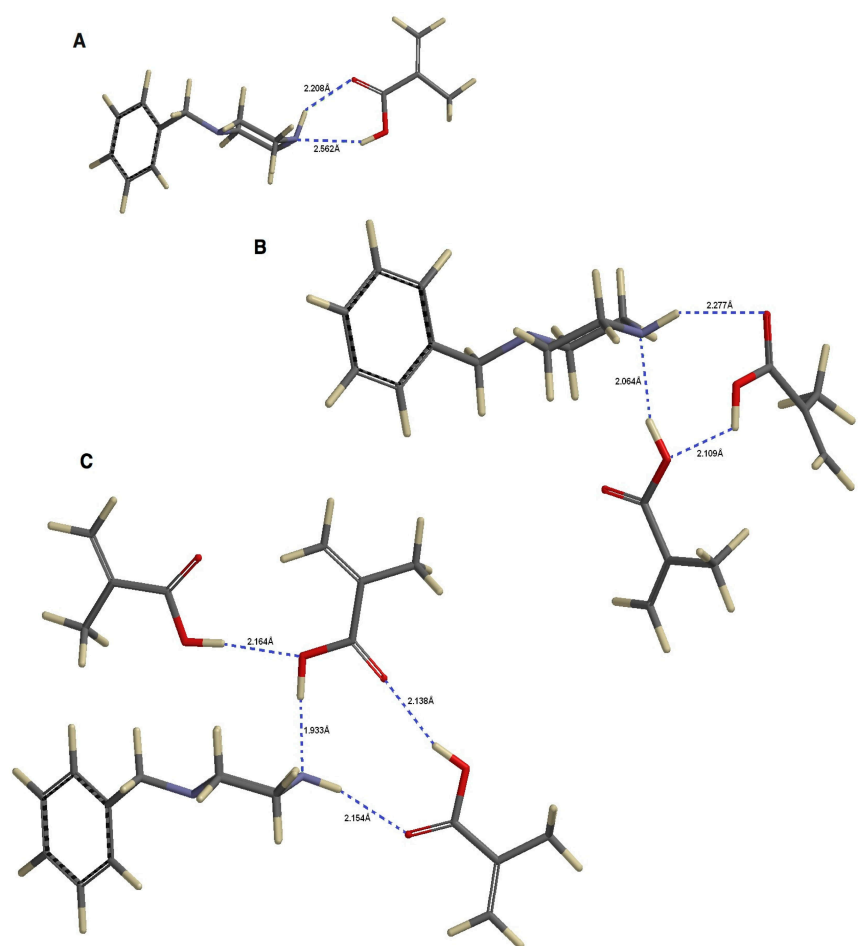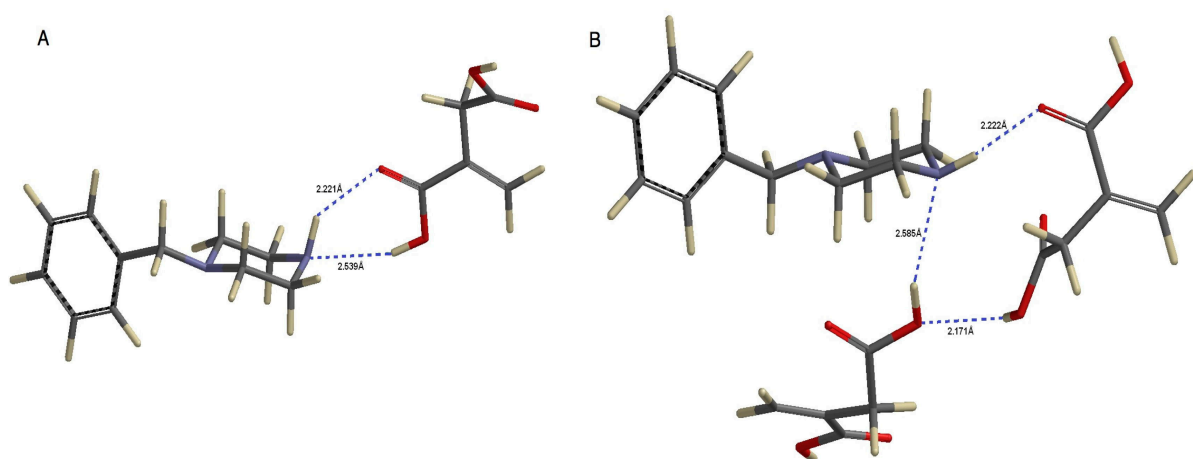
Electronic Supporting Information

Contents

Figure S1. Energy minimised computer modelling representations of the interaction of benzylpiperazine (**1**) with acrylic acid (**6**) in the ratios, **A**) 1:1; **B**) 1:2; and **C**) 1:3.

Figure S2. Energy minimised computer modelling representations of the interaction of benzylpiperazine (**1**) with methacrylic acid (**7**) in the ratios of, **A**) 1:1; **B**) 1:2; and **C**) 1:3.

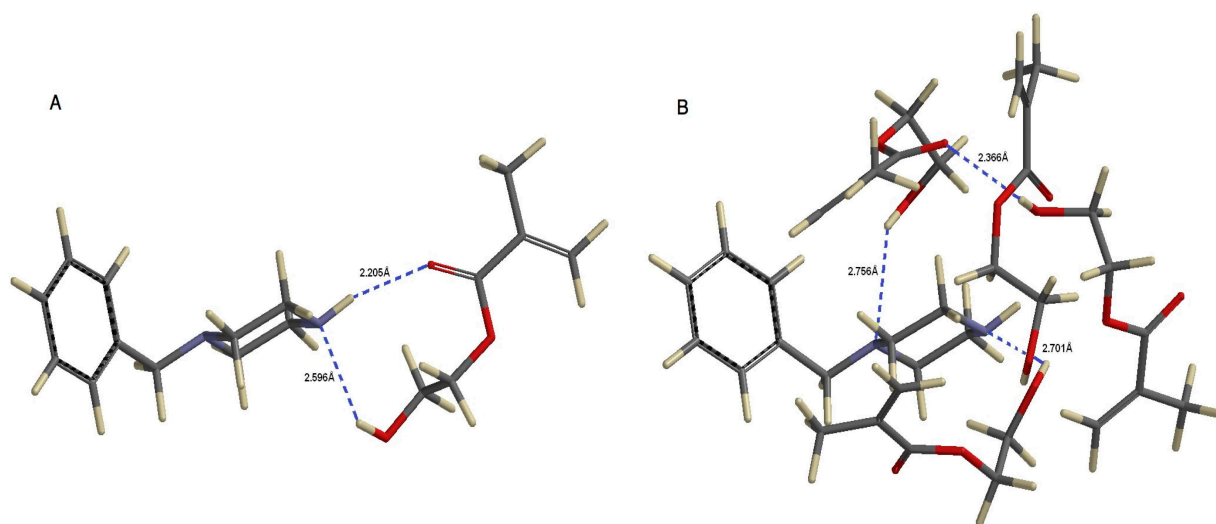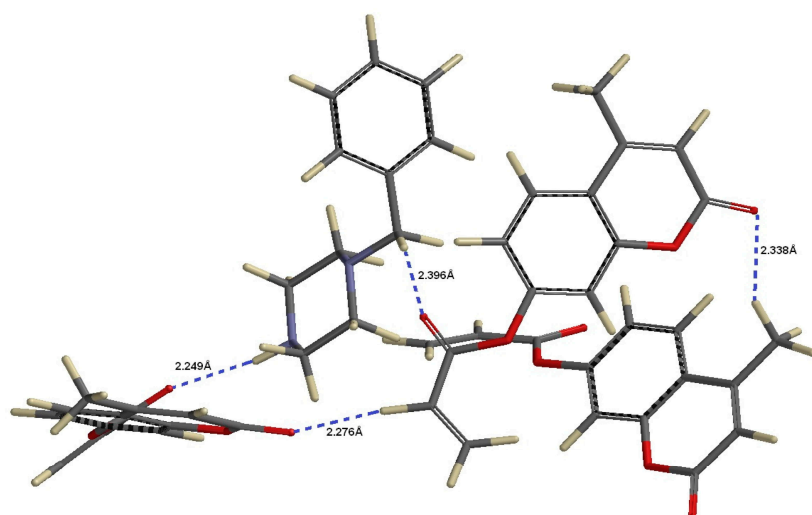**Figure S3.** Energy minimised computer modelling representations of the interaction of benzylpiperazine (**1**) with itaconic acid (**12**) in the ratios of, **A**) 1:1; and **B**) 1:2.

Figure S4. Energy minimised computer modelling representations of the interaction of benzylpiperazine (**1**) with 2-hydroxymethyl methacrylate (**13**) in the ratios of, **A**) 1:1 and **B**) 1:4.

Figure S5. Energy minimised computer modelling representations of the interaction of benzylpiperazine (**1**) with 7-hydroxy-4-methylcoumarin acrylate (**15**) in the ratio of 1:3.

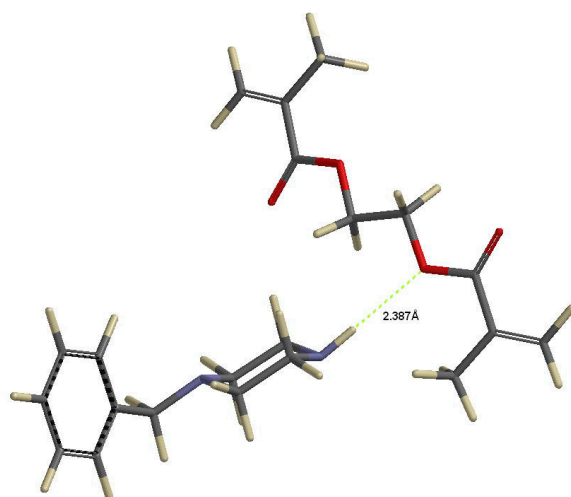**Figure S6.** Energy minimised computer modelling representations of the interaction of benzylpiperazine (**1**) with EGDMA in an optimised 1:1 ratio.

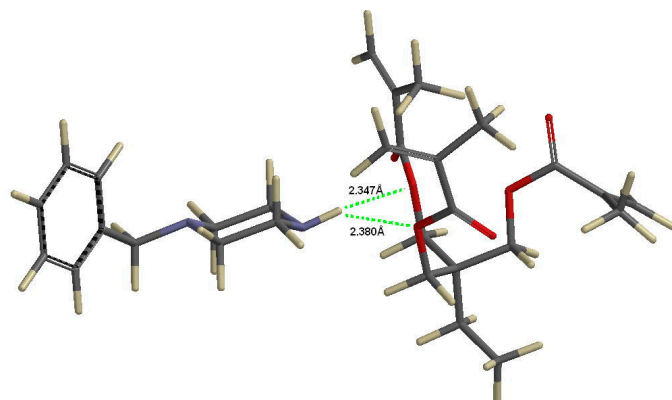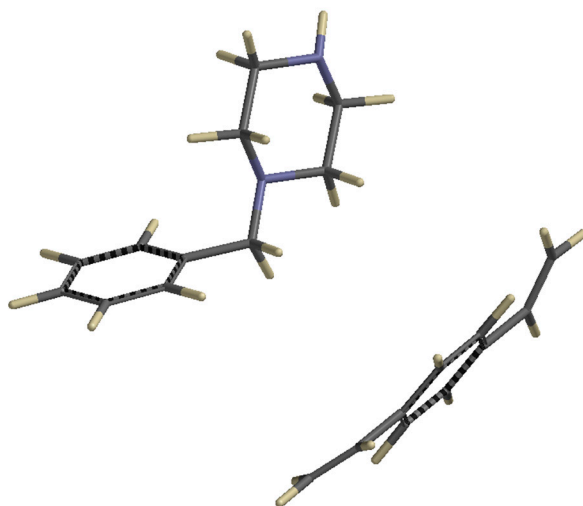**Figure S7.** Energy minimised computer modelling representations of the interaction of benzylpiperazine (**1**) with TRIM in an optimised 1:1 ratio.

Figure S8. Computer generated molecular modelling image for benzylpiperazine (**1**) with divinylbenzene (DVB) for the geometry optimised 1:1 cluster.
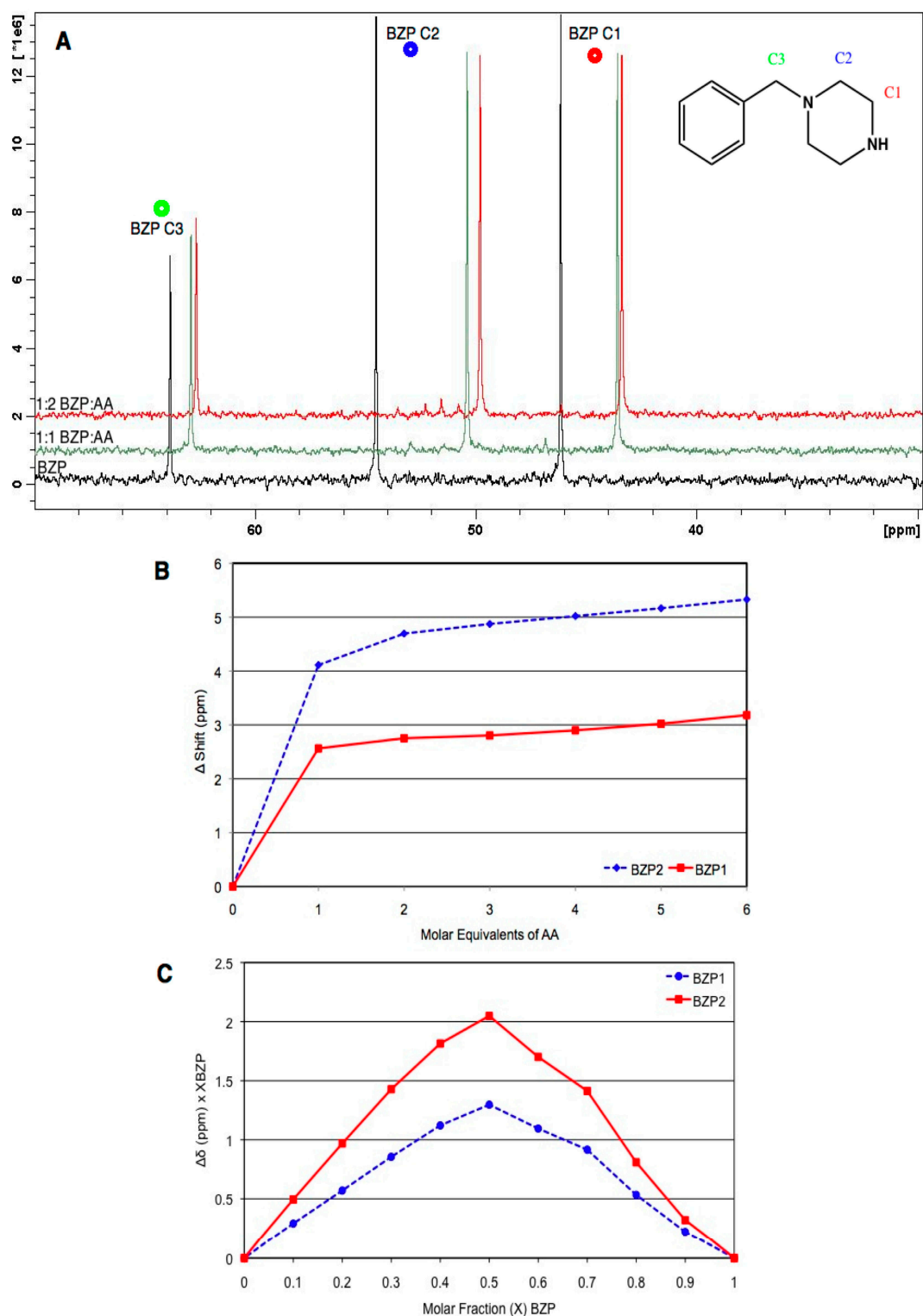
Figure S9. NMR analysis of benzylpiperazine (**BZP**, **1**) with acrylic acid (**AA**, **6**) showing, **A**) the ^{13}C NMR spectra for the NMR titration of **BZP** with **AA** at a T:FM ratio of 1:0, 1:1 and 1:2; **B**) the changes in chemical shift of carbons 1 and 2 on benzylpiperazine (**1**) as a function of increasing **6** concentration; and **C**) Job's plot of two selected **BZP** carbon resonances (C1 and C2) in the presence of **AA**. Cluster stoichiometry is 1:1. ^{13}C NMR spectra obtained at 28 ºC in deuterated chloroform.
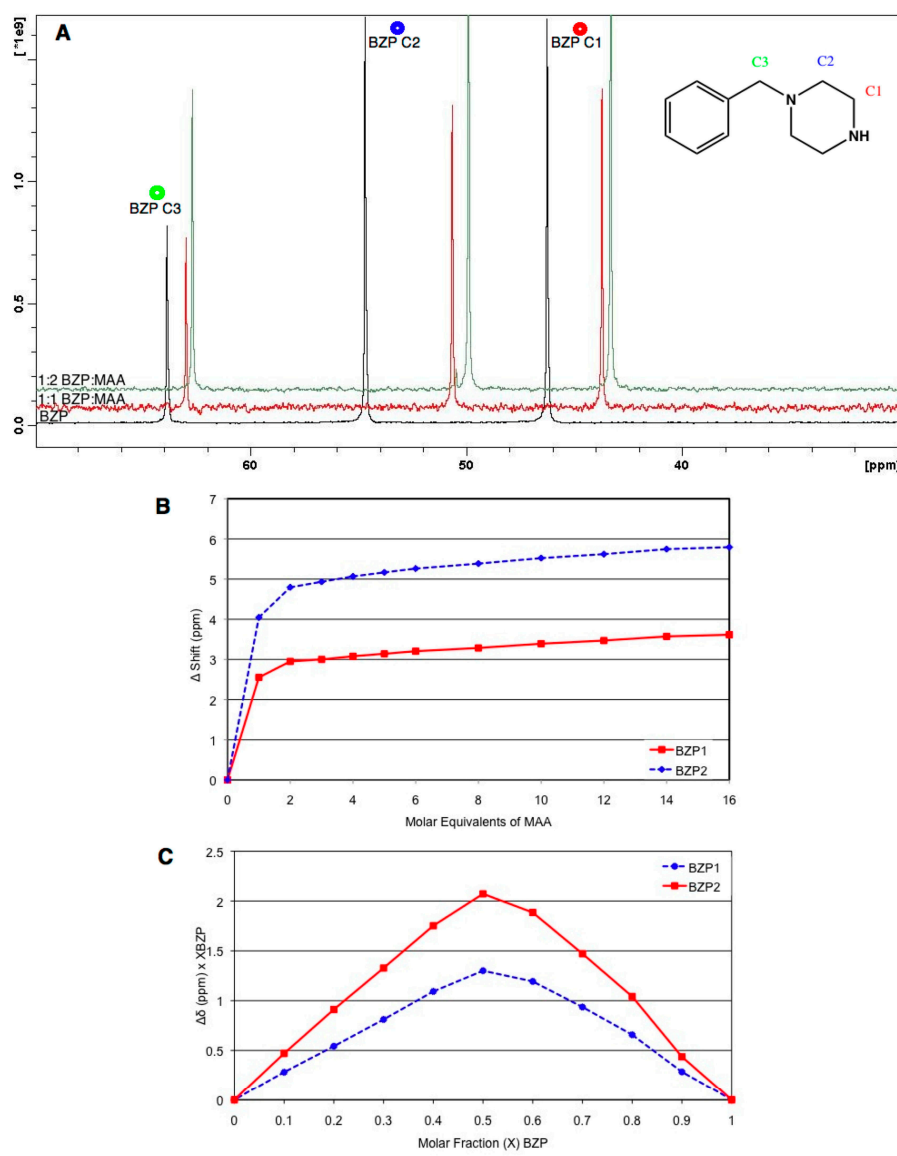
Figure S10. NMR analysis of benzylpiperazine (**BZP**, **1**) with methacrylic acids (**MMA**, **7**) showing, **A**) the ^{13}C NMR spectra for the NMR titration of **BZP** (**1**) with **MAA** (**7**) at a T:FM ratio of 1:0 (no **7** added), 1:1 and 1:2; **B**) the changes in chemical shift of **BZP** carbons 1 and 2 as a function of increasing **MAA** (**7**) concentration; and **C**) Job's plot of two selected **BZP** carbon s (C1 and C2) in the presence of **MAA** showing the predominant cluster stoichiometry as 1:1. ^{13}C NMR spectra obtained at 28 ºC in deuterated chloroform.
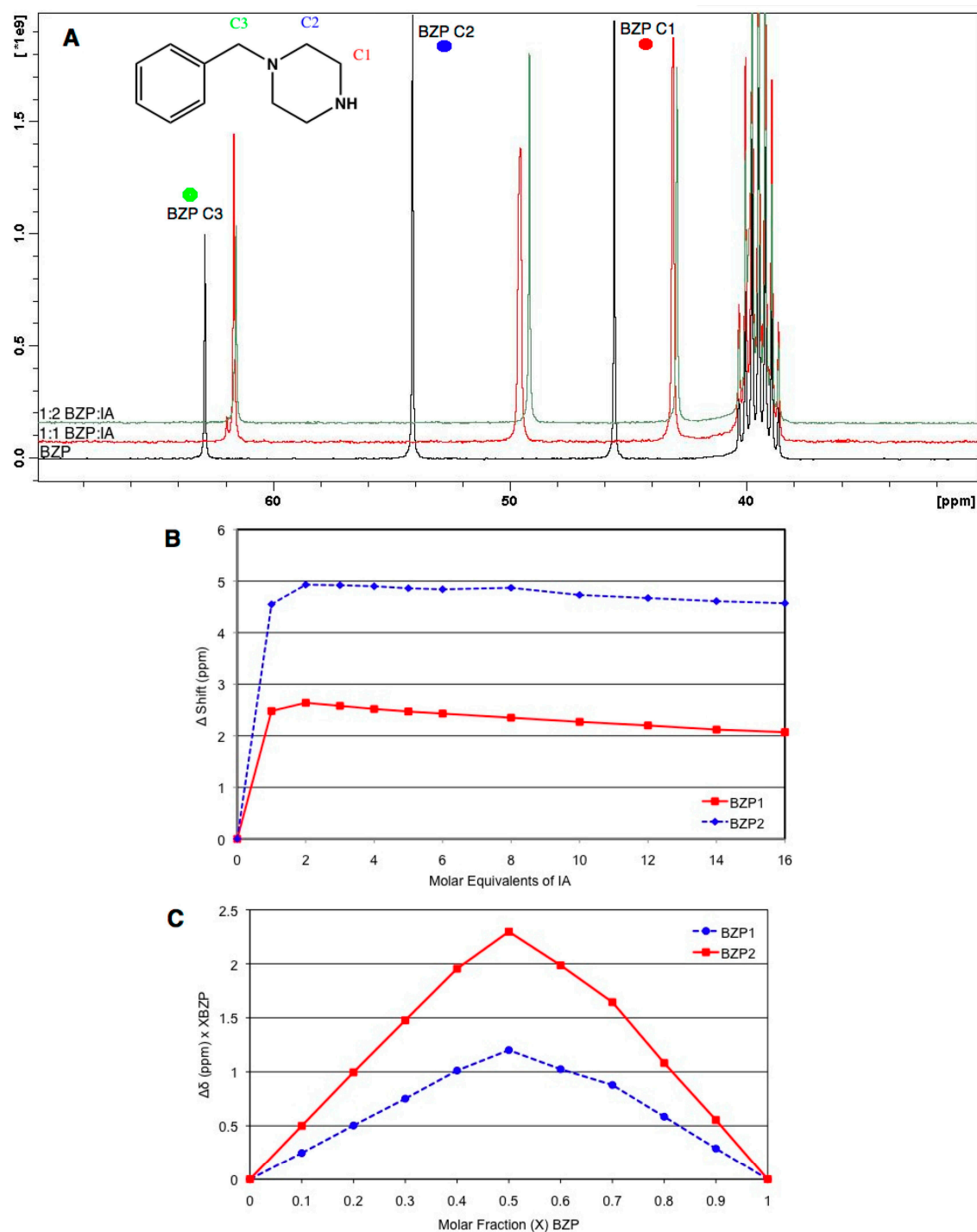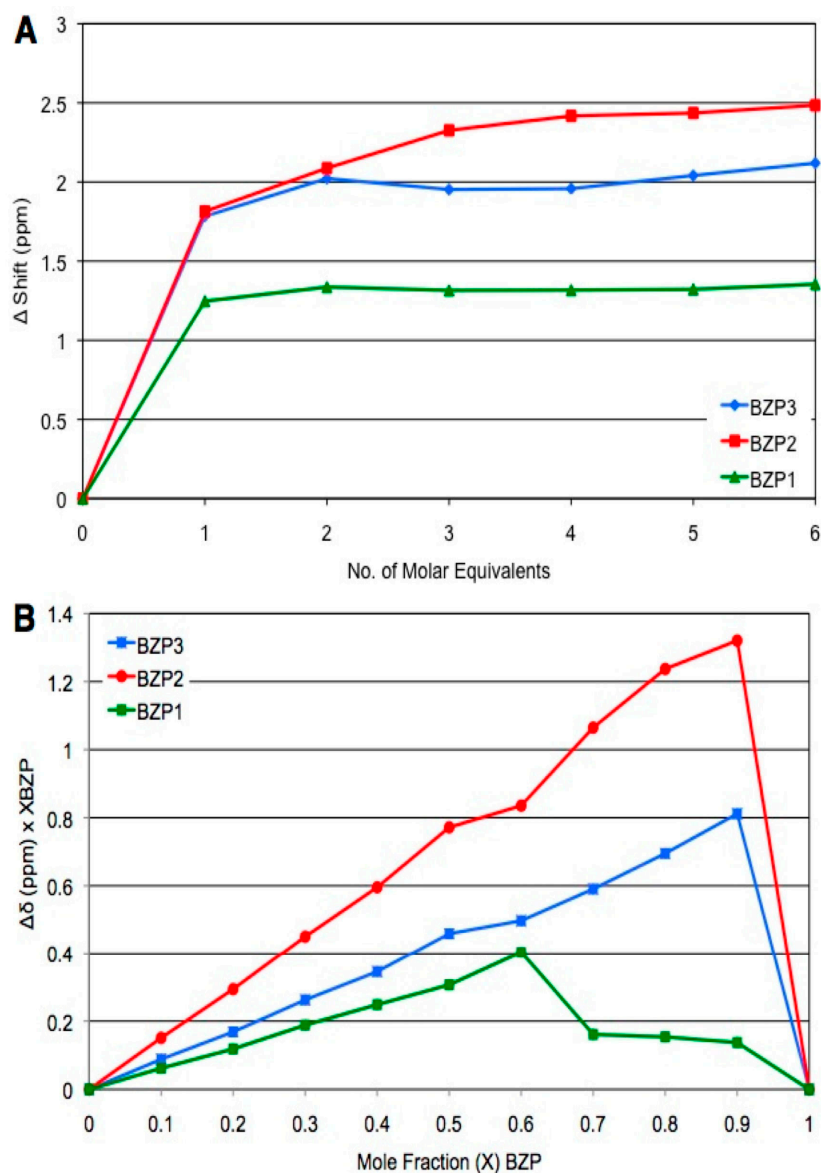
Figure S11. NMR analysis of benzylpiperazine (**BZP**, **1**) with itaconic acid (**IA**, **12**) showing, **A**) the ^{13}C NMR spectra for the NMR titration of BZP (**1**) with IA at a T:FM ratio of 1:0, 1:1 and 1:2 BZP (**1**):IA; **B**) the changes in chemical shift of carbons 1 and 2 on **BZP** as a function of increasing **IA** concentration; and **C**) Job's plot of two selected **BZP** carbon resonances (C1and C2) in the presence of **IA**. Cluster stoichiometry is 1:1. ^{13}C NMR spectra obtained at 28 ºC in deuterated DMSO.

**Figure S12.** NMR analysis of benzylpiperazine (**BZP**, **1**) with 7-hydroxy-4-methylcoumarin acrylate (**HMCA**, **15**) showing, **A)** the changes in chemical shift of carbons 1 and 2 on **BZP** as a function of increasing **HMCA** concentration; and **B)** Job's plot of two selected benzylpiperazine (**1**) carbon resonances (C1 and C2) in the presence of HMCA. Cluster stoichiometry was 9:1 **BZP:HMCA**. ^{13}C NMR spectra obtained at 28 ºC in deuterated chloroform.
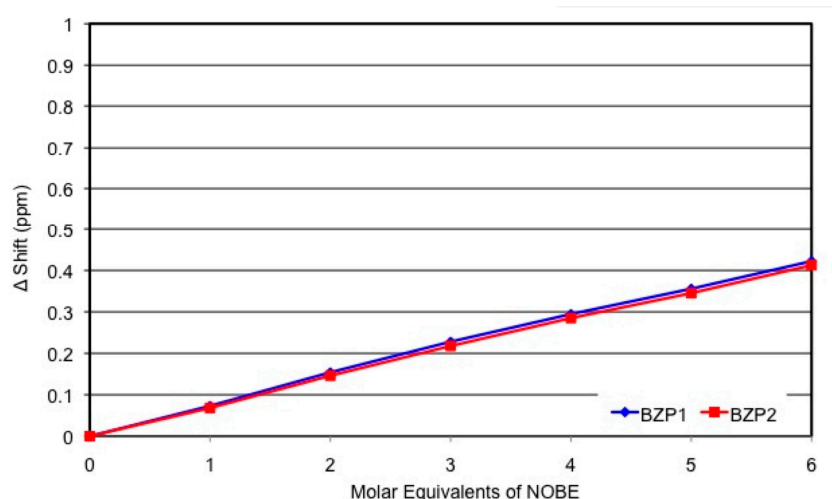
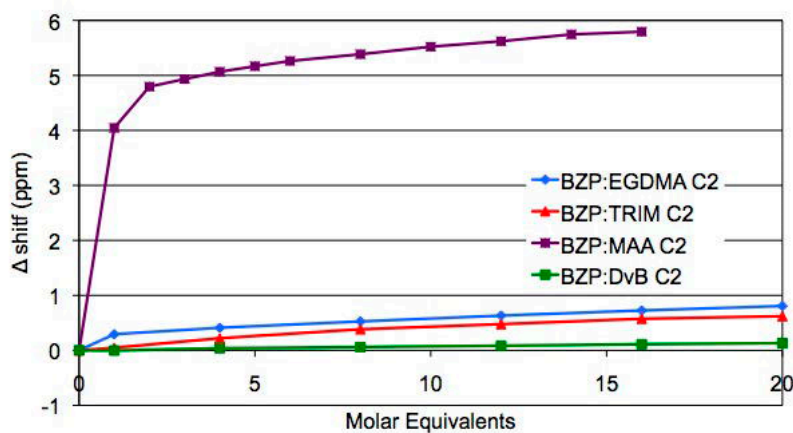**Figure S13.** NMR titration of benzylpiperazine (**BZP**, **1**) with N,O-bismethacroyloyl ethanolamine (**NOBE**, **14**) showing the changes in chemical shift of carbons 1 and 2 on **BZP** as a function of increasing **NOBE** concentration.
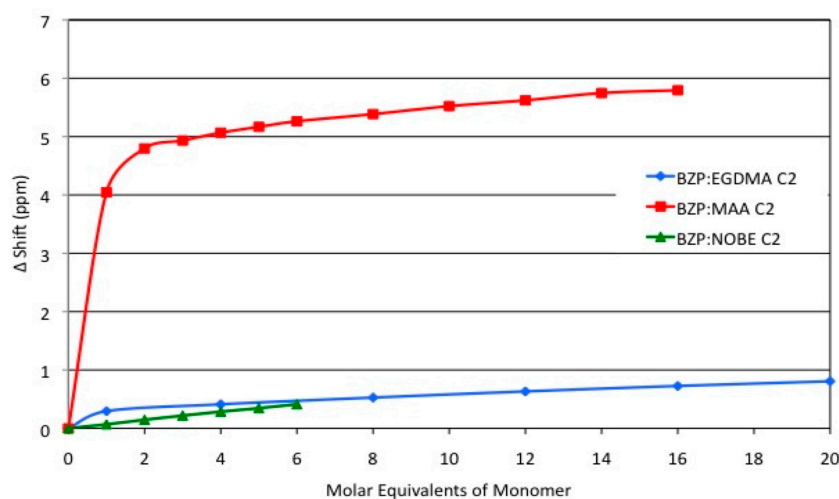

Figure S14. NMR titration of benzylpiperazine (**BZP**, **1**) with N,O-bismethacroyloyl ethanolamine (**NOBE**, **14**), methacrylic acid (**MAA**, **7**) and ethylene glycol dimethylacrylate (**EGDMA**) showing the changes in chemical shift of carbon 1 on **BZP** as a function of increasing monomer concentration.


Figure S15. NMR titration of benzylpiperazine (**BZP**, **1**) with ethylene glycol dimethylacrylate (**EGDMA**), trimethylolpropane trimethylacrylate (**TRIM**), divinylbenzene (**DVB**) and methacrylic acid (**MAA**, **7**) showing the most significant change in chemical shift experienced as a function of increasing **EGDMA**, **TRIM**, **DVB** and **MAA** concentration, respectively. **MAA** has been included for comparison
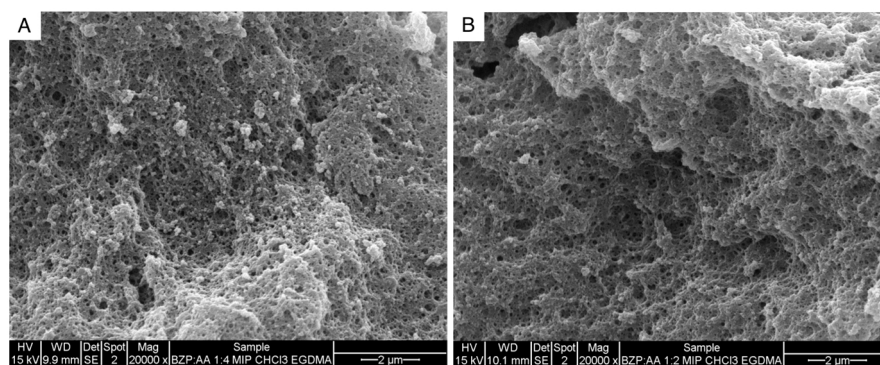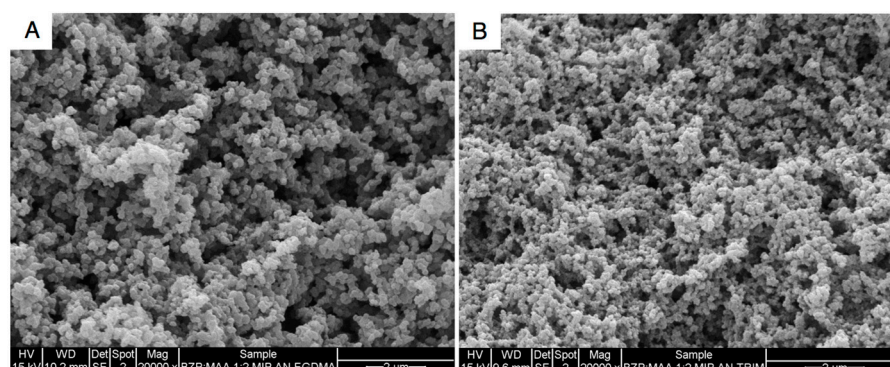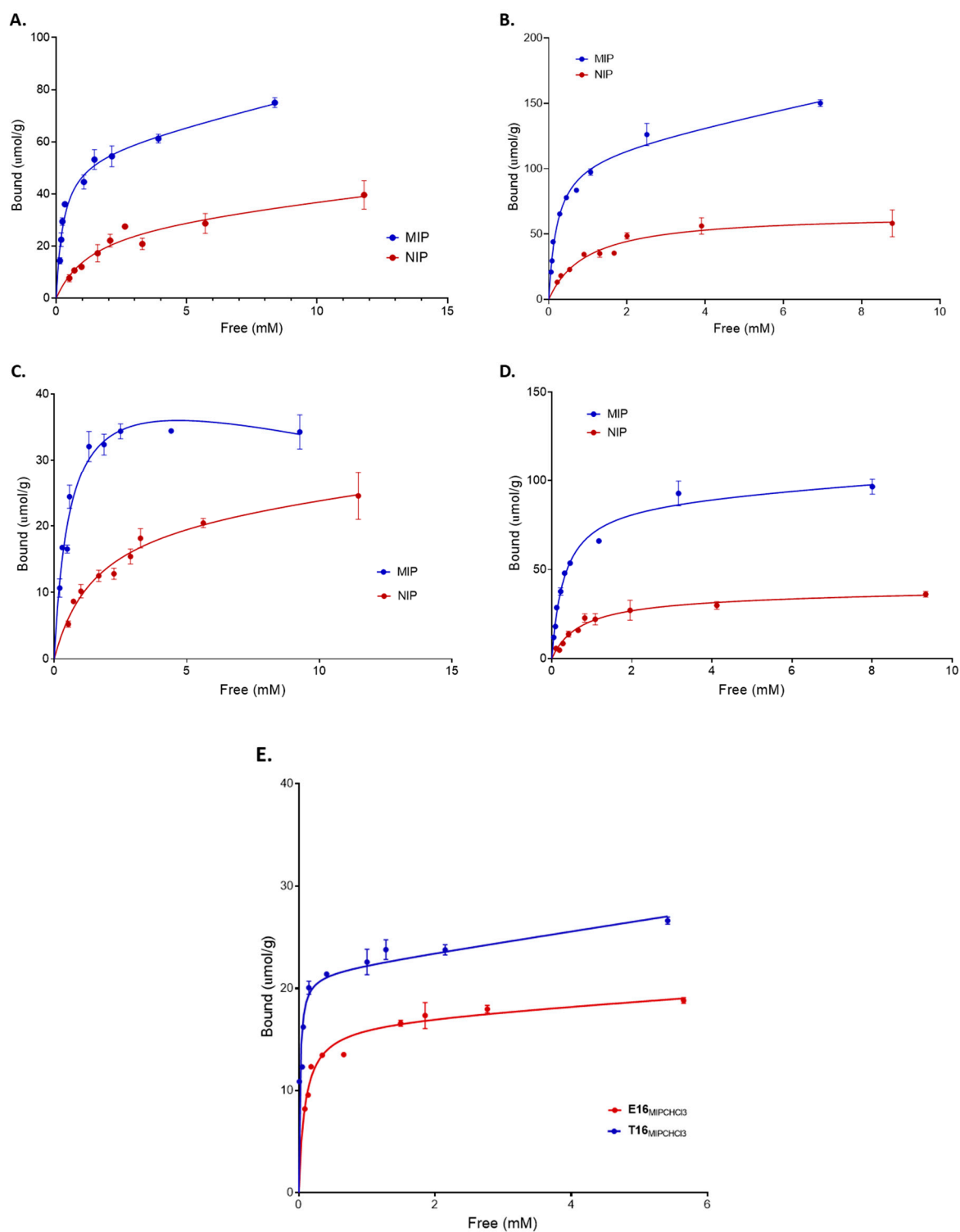
Figure S16. SEM images for A) $E6_4$-MIP$_{CHCl3}$ and B) $E6_2$-MIP$_{CHCl3}$ MIPs obtained at 20000x magnification at 15.0 kV.
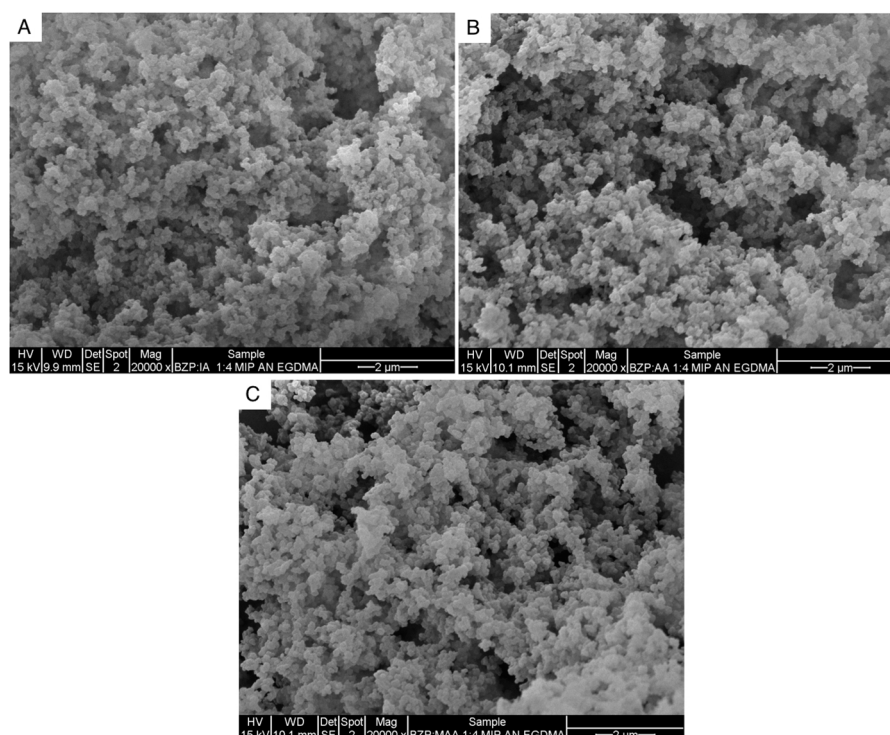
Figure S17. SEM images for A) $E12_4$-MIP$_{CH3CN}$, B) $E6_4$-MIP$_{CH3CN}$ and C) $E7_4$-MIP$_{CH3CN}$ MIPs obtained at 20000x magnification at 15.0 kV.
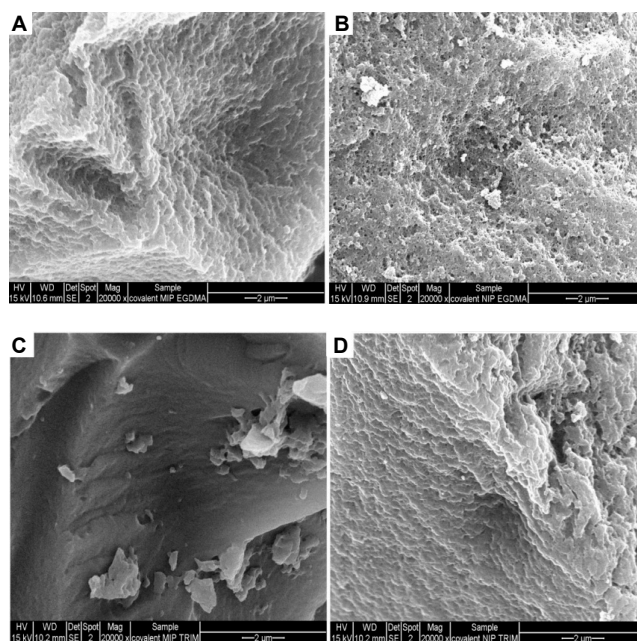

Figure S18. SEM images for A) $E7_2$-MIP$_{CH3CN}$, and B) $T7_2$-MIP$_{CH3CN}$ MIPs obtained at 20000x magnification at 15.0 kV.

Figure S19. Binding isotherms produced for (**A**) E7$_{1\text{-MIPCHCl3}}$; (**B**) E7$_{2\text{-MIPCHCl3}}$; (**C**) T7$_{1\text{-MIPCHCl3}}$; and (**D**) T7$_{2\text{-MIPCHCl3}}$ and (**E**) semi-covalent E16$_{\text{MIPCHCl3}}$ and T16$_{\text{MIPCHCl3}}$.

Figure S20. SEM images for (**A**) E16$_{MIPCHCl3}$, (**B**) E$_{NIP}$, (**C**) T16$_{MIPCHCl3}$ and (**D**) T$_{NIP}$.
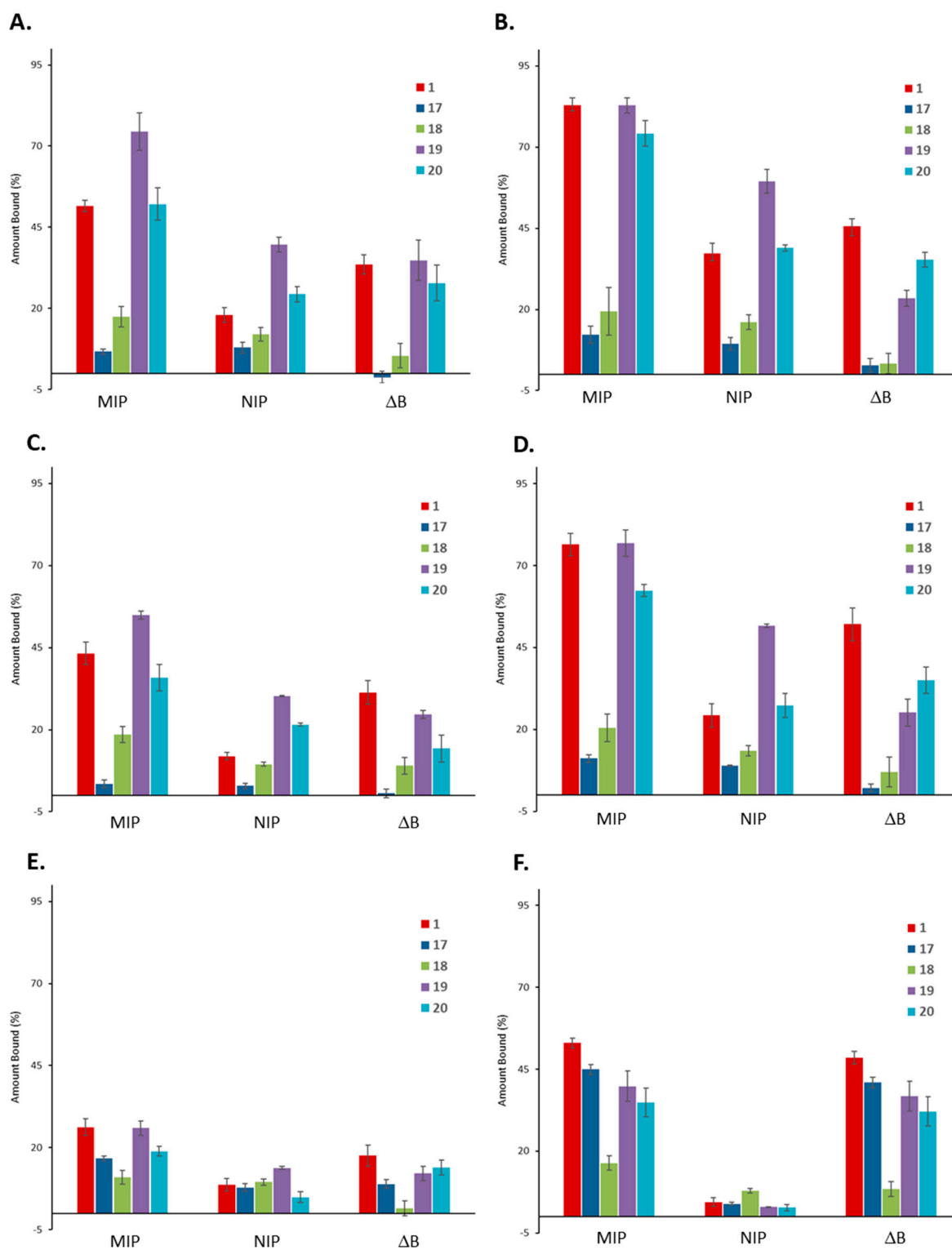
Figure S21. Cross-reactivity data for (**A**) E7$_{1\text{-MIPCHCl3}}$; (**B**) E7$_{2\text{-MIPCHCl3}}$; (**C**) T7$_{1\text{-MIPCHCl3}}$; (**D**) T7$_{2\text{-MIPCHCl3}}$; (**E**) E16$_{\text{MIPCHCl3}}$; and (**F**) T16$_{\text{MIPCHCl3}}$ using 20 mg of polymer and 0.8 mM analyte solutions at t = 60 min in triplicate.
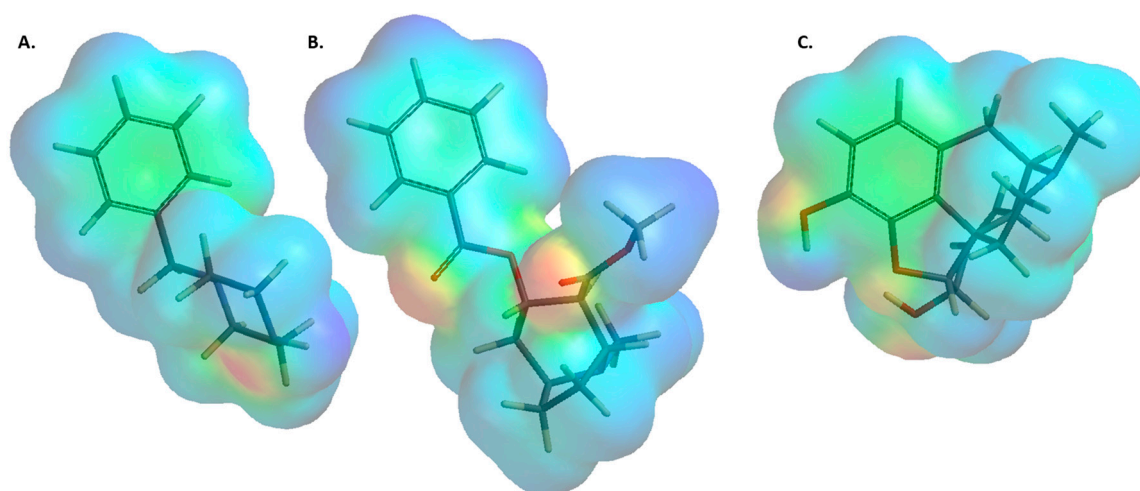
Figure S22. Molecular modelling images of **1** (**A**), **17** (**B**) and **18** (**C**) showing their differences in surface potential and size.
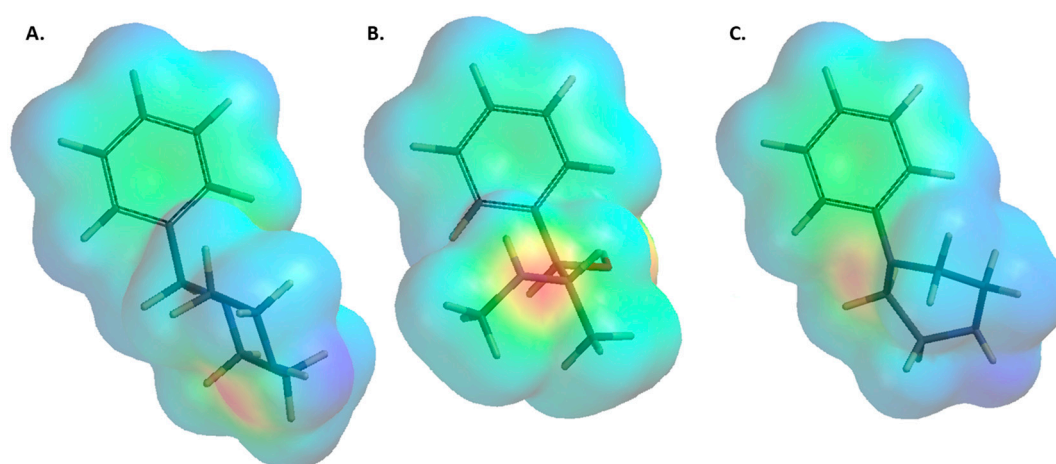
Figure S23. Molecular modelling images of **1** (**A**), **19** (**B**) and **20** (**C**) showing their similarities in surface potential and size.
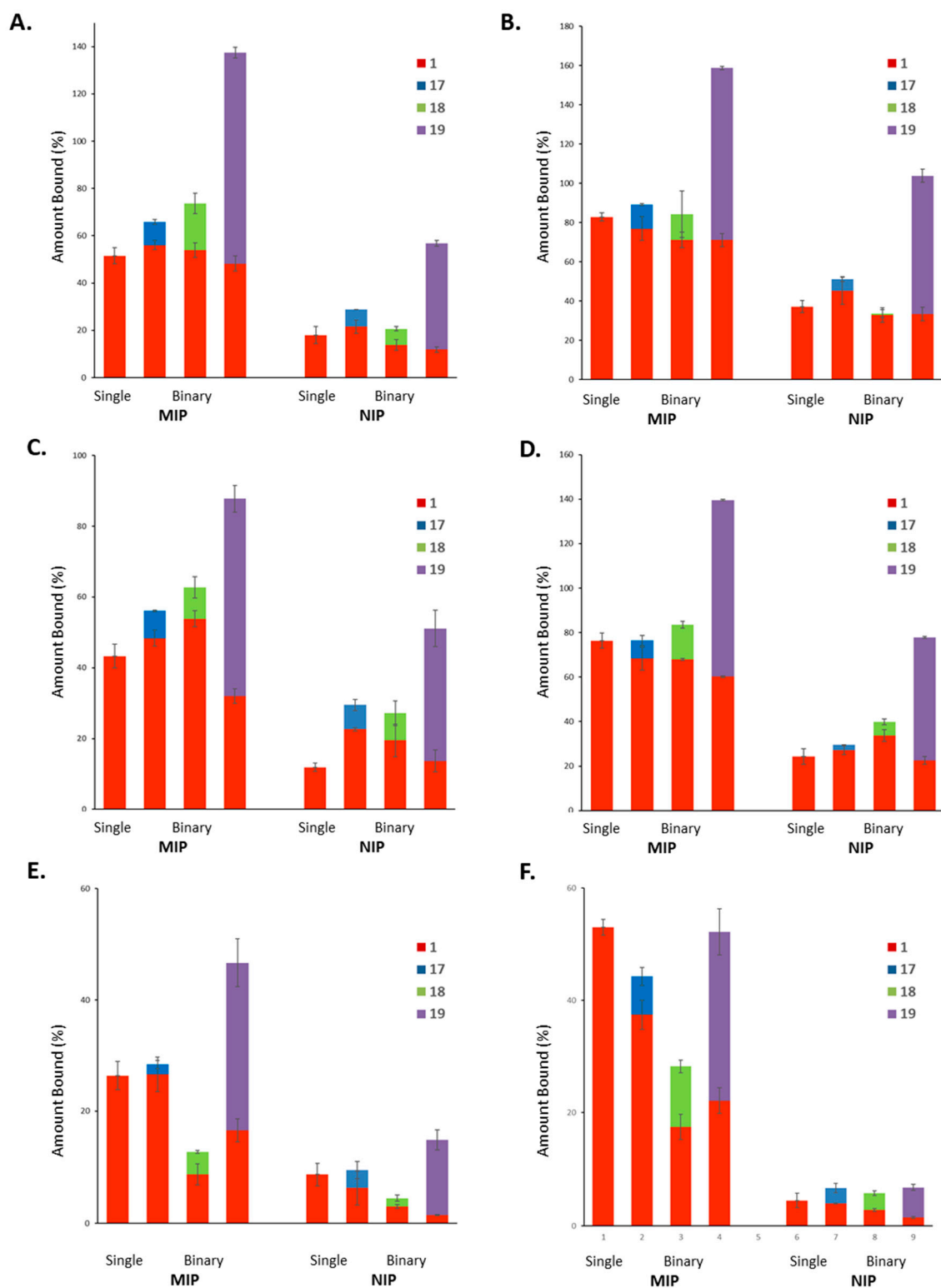
Figure S24. Competitive binary binding data for (**A**) E7$_{1\text{-MIPCHCl3}}$; (**B**) E7$_{2\text{-MIPCHCl3}}$; (**C**) T7$_{1\text{-MIPCHCl3}}$; (**D**) T7$_{2\text{-MIPCHCl3}}$; (**E**) E16$_{\text{MIPCHCl3}}$; and (**F**) T16$_{\text{MIPCHCl3}}$ using 20 mg of polymer and a mixture of 0.8 mM solution of **1** and 0.8 mM solution of analyte (**17**, **18** or **19**) at t = 60 min in triplicate. Binding is expressed in % with respect to the original concentration; for a binary system, this would translate to values higher than 100%.